Fourier microfluidics†

Y. Xie, Y. Wang, L. Chen and C. H. Mastrangelo

Received 30th November 2007, Accepted 19th February 2008
First published as an Advance Article on the web 13th March 2008
DOI: 10.1039/b718376c

We present a new experimental technique for the separation of dynamic chemical signals based on their frequency domain characteristics. Such a technique can be used to create filters that separate slow signals from fast signals from a common input flow stream. The propagation of time-varying chemical waves through networks of microfluidic channels is first examined. Mathematical models and a set of simple experiments are developed that demonstrate that short microfluidic channels behave as linear delay lines. The observed dispersive broadening and delay behavior can be explained in Fourier space in terms of corresponding phase delay, amplitude decay and characteristic transfer functions. Such delay components can be utilized to implement frequency dependent interference filters. An 8th order PDMS bandpass filter chip demonstrating these ideas was constructed. The filter chip has a central frequency of 0.17 Hz and a bandwith of 0.04 Hz at a flow rate of 4 μL h^{-1}.

Introduction

Dynamic chemical signals are pervasive in biology.[1,2] For example, chemical signals control biological processes in protein activation and signaling,[3–9] paracrine and endocrine cell-to-cell communication,[10–13] inflamatory response,[14–16] and regulate many aspects of stem-cell growth and tissue differentiation.[17] The time scales for many of these signals range from a fraction of a second to several minutes.

In spite of their relevance, there are no well established techniques for analysis and separation of time-dependent signals. Conventional chemical analysis techniques such as electrophoresis and liquid chromatography can only be used for the analysis of finite, discrete and time invariant samples; hence many samples must be collected to determine the dynamic nature of a signal.

In this paper, we report an experimental technique that separates chemical signals based not on their chemical nature but their Fourier, frequency-domain characteristics. Fourier methods have been previously utilized for rear analysis in capillary electrophoresis,[18] measurement of electrokinetic velocity,[19] and as a method for separation of different species in cyclic electrophoresis.[20,21] In the technique described here we introduce the concept of microfluidic Fourier filters. Fourier filters transmit frequency-specific signals rejecting all others. With such filters one could separate slow signals from fast signals carried in a common input stream as shown in Fig. 1. The input stream could originate for example from a time-dependent cellular release, or *in-vitro* experiments of protein signalling networks.

In the sections below we demonstrate how these filters can be implemented using a simple array of microfluidic channels that in Fourier space map directly to elementary filter components. Using these elementary components we designed and constructed a bandpass filter implemented with PDMS chips.

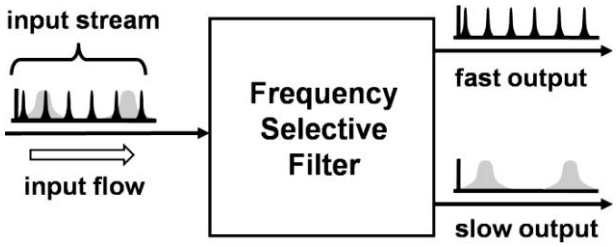

Fig. 1 Separation of fast and slow chemical signals carried by a common input stream. The frequency selective filter splits the flow into two outputs corresponding to slow and fast signals.

Propagation of periodic signals in microchannels

In order to explain these concepts we first examine the propagation of a periodic chemical signal flowing through a simple microfluidic channel of uniform cross section as shown in Fig. 2(a). The microchannel is excited with a signal generator consisting of four valves (shown as switches) driven by digital clock signals ϕ and $\bar{\phi}$. The generator maintains a constant flow of alternating analyte or solvent (H_2O) at excitation frequency $\omega = 2\pi\tau^{-1}$ introducing a periodic analyte pulse train into the channel.

As this signal travels through the channel the analyte pulses are both broadened by Taylor dispersion[1] and delayed in time. If the transit time is sufficiently long, the dispersive broadening eventually produces overlapping pulses and a net reduction of the concentration variation. The presence of these effects is observed in the experimental results of Fig. 2(b) showing the propagation of fluorescein disodium (1 mg mL^{-1}) waves at different distances from the inlet of a PDMS channel under typical flow conditions. The recorded waves, averaged across the channel cross section, exhibit both delay and amplitude attenuation characteristics of dispersion. Further, the longer the distance from the inlet, the more the signal resembles a pure sinusoidal.

Electrical Engineering and Computer Science Department, Case Western Reserve University, Cleveland, OH, USA.
E-mail: yxx15@case.edu, carlos.mastrangelo@case.edu

† Electronic supplementary information (ESI) available: Mathematical model for propagating waves. See DOI: 10.1039/b718376c

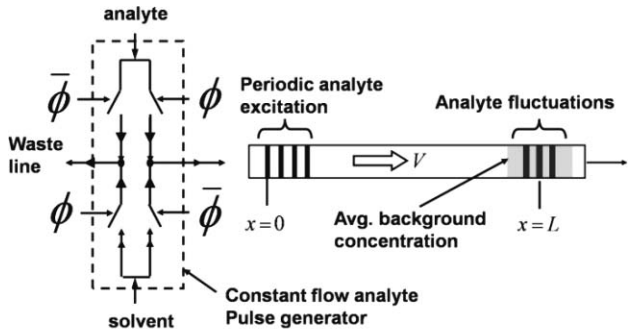

(a)

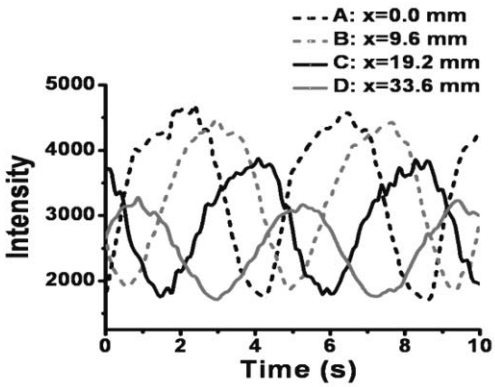

(b)

Fig. 2 (a) Microfluidic circuit for injection of periodic analyte excitation into a channel. Analyte waveforms are delayed and dispersed as they travel to the channel output. (b) Observed fluorescein waveforms at different distances downstream from a PDMS channel inlet (25 × 16 μm^2 at average velocity ~1 cm s^{-1}). The measurement spot was 25 × 25 μm^2.

All of these observations can be predicted using the following mathematical model. From first principles, the propagating signal is represented by a space and time dependent concentration $c(x,y,z,t)$ of a dilute solute flowing through the channel with velocity $v(y,z)$ where $0 \le z \le h$ and $0 \le z \le w$ are coordinates normal and parallel to the channel substrate, and x is the coordinate along the flow direction. The solute concentration is periodic $c(x,y,z,t) = c(x,y,z,t+\tau)$, and it obeys a complex four dimensional convection diffusion PDE.[22] However if the channel height h and width w are small relative to its length L, we can considerably simplify the problem if one considers the behavior of the average concentration $C(x,t)$ across its cross section under the influence of its average velocity V where

$$C(x,t) = \frac{1}{wh}\int_0^w\int_0^h c(x,y,z,t)\,dy\,dz, \qquad V = \frac{1}{wh}\int_0^w\int_0^h v(y,z)\,dy\,dz \tag{1}$$

The average concentration $C(x,t)$ is also periodic $C(x,t) = C(x,t+\tau)$, and it approximately obeys the simplified, lumped one-dimensional convection–diffusion equation

$$D\frac{\partial^2 C}{\partial x^2} - V\frac{\partial C}{\partial x} = \frac{\partial C}{\partial t} \tag{2}$$

where D is the effective diffusion constant adjusted for Taylor-dispersion.[23] In Fourier space we can represent the average signal as $C(j\omega,x)$; hence the time derivative term in eqn (2) is readily replaced with the complex term $j\omega C$.

$$D\frac{d^2C}{dx^2} - V\frac{dC}{dx} = j\omega C \tag{3}$$

Solving this ODE with suitable boundary conditions $C(j\omega,0) = C_{in}(j\omega)$ and $C(j\omega,\infty) = 0$ one obtains the transfer function (TF) $T(j\omega,x)$ for the microfluidic channel

$$T(j\omega,x) = C_{out}(j\omega,x)/C_{in}(j\omega) = \exp[(V - \sqrt{V^2 + 4j\omega D})x/2D] \tag{4}$$

where x is the distance measured from the channel inlet.

While at first the behaviour of the complex exponential in eqn (4) is difficult to ascertain, it becomes very clear when we plot the magnitude $\|T(j\omega,x)\|$ *versus* frequency as shown in the Bode plot of Fig. 3(a).

At low excitation frequencies the pulse distortion and amplitude decay are minimal yielding a near flat TF regime, but beyond a cut off frequency ω_c the amplitude attenuation is very large. A simple second order Taylor expansion of eqn (4) yields the approximate cut off frequency

$$\omega_c \approx \left[\frac{V^3}{DL}\right]^{1/2} \tag{5}$$

where D is the corresponding dispersion adjusted diffusion constant[23–27] which depends on velocity and capillary cross section dimensions.

At low frequencies and for short channels the amplitude decay is negligible, and eqn (4) simply reduces to

$$T(j\omega,x) \approx \exp[-j(\omega x/V)] = \exp(-j\theta) \tag{6}$$

where

$$\theta = \frac{\omega x}{V} = \omega T = \frac{2\pi x}{\lambda} \tag{7}$$

is a characteristic phase delay angle proportional to the signal transit time $T = x/V$ and input frequency ω, and λ is the characteristic wavelength. Short channels in the flat regime therefore act as elementary delay line elements with phase angle linearly proportional to their length. On the other hand, long channels behave as low-pass filter elements that time average (and mix) the incoming pulses reducing the overall amplitude. In addition, since the propagating signal is periodic, it can also be expressed as a Fourier series. Very long channels strongly attenuate all of the high frequency series components basically leaving only the average and the first (fundamental) term of the series. This low-pass filter action explains why the observed output signal in Fig. 2 (see signal D) converges to a simple sinusoidal wave at the fundamental frequency.

Interference of chemical waves

A basic phenomenon required for the realization of Fourier filters is linear interference. If two zero-average periodic signal excursions of same excitation frequency but differing by phase

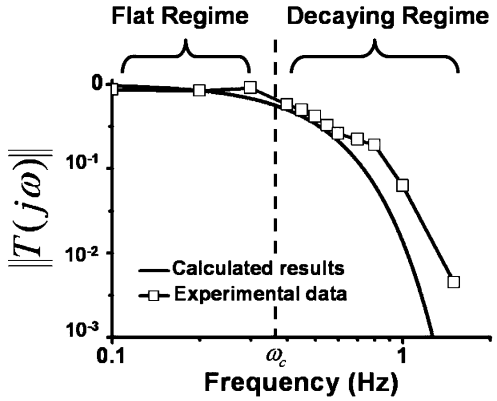

(a)

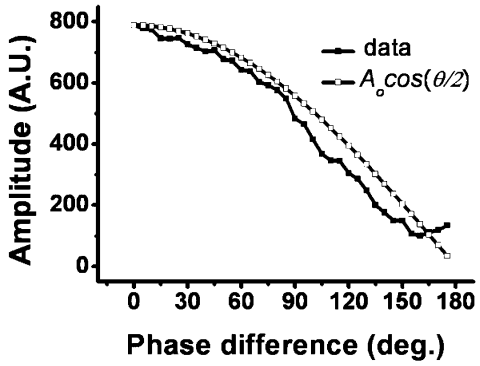

(b)

Fig. 3 (a) Observed and calculated transfer function magnitude *versus* excitation frequency at 19.2 mm downstream from a PDMS channel inlet. The cross section of the channel was 25 × 16 μm² and the flow velocity was 1 cm s⁻¹. (b) Observed averaged signal amplitude at the fundamental frequency *versus* phase in a PDMS channel driven by two signal generators out of phase. The flow rate for this experiment was 0.8 cm s⁻¹ at 0.5 Hz with a microfluidic channel cross section dimension of 25 × 16 μm². The measurement spot was 25 × 25 μm².

θ are added at a common node, the resulting waveform should obey the linear interference identity

$$A\cos(\omega t) + A\cos(\omega t + \theta) = 2A\cos(\omega t + \frac{\theta}{2})\cos(\frac{\theta}{2}) \quad (8)$$

The right hand side contains the product of a time-varying and a fixed term. If the phase difference is zero the two signals add up constructively, but when $\theta = \pi$ the two signals cancel out. Linear interference was tested using a PDMS chip consisting of not one but two signal generators connected to a simple microchannel. The amplitude of the observed response, averaged across the cross section, was next recorded when the two generators were driven at the same excitation frequency but with different phase. The amplitude of the combined measured signal at the fundamental frequency is shown in Fig. 3(b), indicating that it follows eqn (8) closely and linear interference holds.

This plot represents the amplitude of excursions above the input average. If the two generators are driven exactly out of phase the combined signal is exactly equal to this average and the amplitude of the excursion is exactly zero.

We now have sufficient knowledge and suitable models of chemical wave propagation through these systems to implement a variety of Fourier filters.

*N*th order ideal bandpass filters

Since chemical signals can be added constructively or destructively depending on their relative phase, we can create a wide variety of frequency selective filters using functions of the type

$$T_F(j\omega) = \sum_{i=1}^{N} A_i e^{-j\theta_i} \quad (9)$$

where A_i are leading weight constants and θ_i are frequency dependent phase terms. Such a function is easily implemented with a network of delay elements (short microchannels) connected to a common output node. In particular, one can implement sharp bandpass filters with a network of equally weighting channels with channel lengths differing by exactly L as shown in Fig. 4(a).

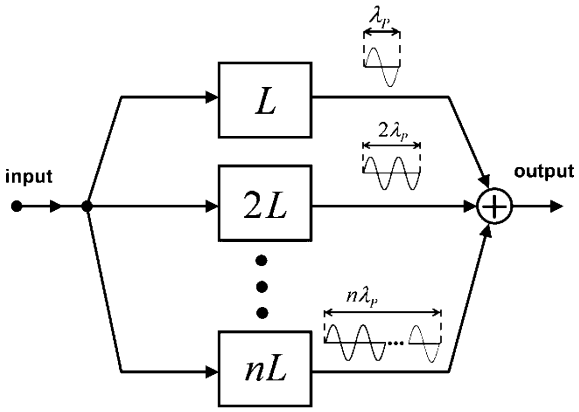

(a)

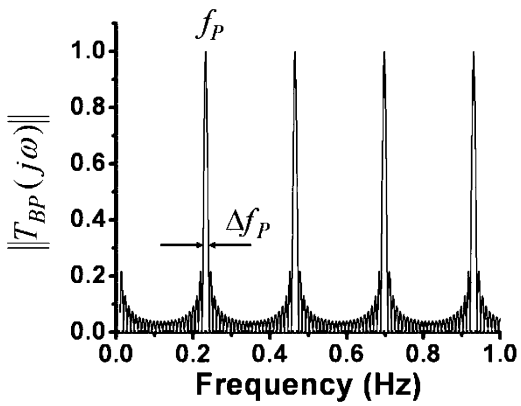

(b)

Fig. 4 (a) Schematic of an *N*th-order bandpass filter. Each delay element consists of a microfluidic channel whose length differs from the next by an integer number of wavelengths at the central frequency. (b) Plot of idealized transfer function for a band pass filter with $N = 25$ (25 parallel channels) with a flow velocity of 0.15 cm s⁻¹ and with $L =$ 0.7 cm.

The operation of this filter configuration is easy to explain. For most input excitation frequencies the output signals from each element will interfere at the output with uncorrelated phase destructively producing a low output amplitude. However at specific frequencies when the wavelength is equal to an integer of the interchannel spacing $\lambda_P = mL$, all of these signals will add up in phase constructively producing a very sharp output amplitude peak.

The ideal transfer function of the bandpass filter is then

$$T_{BP}(j\omega) = \frac{1}{N}\sum_{n=1}^{N} e^{-j2\pi f^* n} = \frac{1}{N} e^{-j\pi f^*(N+1)} \times \frac{\sin(\pi f^* N)}{\sin(\pi f^*)} \quad (10)$$

with

$$f^* = \frac{f}{(V/L)} = \frac{f}{f_P} \quad (11)$$

where $\omega = 2\pi f$ and $f_P = V/L$ is the peak frequency. The ratio of the two sine functions in eqn (10) generates sharp peaks at integers of f_P. Fig. 4(b) shows the plot of $\|T_{BP}(j\omega)\|$ for $N = 25$. Note that the peaks are band selective, but also periodic so there is a finite range that produces non-overlapping peaks (for $0 < f^* < 1$). The filter sharpness and frequency bandwidth is equal to the width of the main lobe $\Delta f_P = 2f_P/N$; therefore the higher the number of terms in the sum (the filter order) the sharper the filter peak is. The ratio $(f_P/\Delta f_P) = N/2$ also specifies the number of distinct frequency bands that could be separated.

Filter design and feasibility region

The idealized TF of eqn (10) ignores the attenuation effects of dispersion. Minimization of signal attenuation is critically important for a successful bandpass filter design. In order to find suitable filter parameters for low attenuation filter designs, we first rewrite eqn (4) in the following form

$$T(j\omega, x) = \exp(\beta x) = \exp(-x/L_D)\exp[-j\gamma(\omega)x] \quad (12)$$

where

$$\beta = (V - \sqrt{V^2 + 4j\omega D})/2D = \frac{V}{2D}[1 - (1 + 4j\omega D/V^2)^{1/2}] \quad (13)$$

In eqn (12), the $\exp(-x/L_D)$ term yields the amplitude decay, and L_D is a characteristic decay length. The second term $\exp(-j\gamma(\omega)x)$ represents a pure phase shift. When $|4j\omega D/V^2| \ll 1$ the parameter β can be expressed as a second order Taylor series and further simplified to

$$\beta \approx -j\left(\frac{\omega}{V}\right) - \left(\frac{\omega^2 D}{V^3}\right) = -j\gamma(\omega) - \left(\frac{1}{L_D}\right) \quad (14)$$

Thus the decay length L_D is frequency dependent

$$L_D = \frac{V^3}{\omega^2 D} \quad (15)$$

In order to avoid significant amplitude decay at the first peak f_P, we must use channel lengths much smaller than $L_D(f_P)$. In particular, we are interested in the number of wavelengths N_λ that can be fitted within $L_{max} = L_D/m$. To obtain negligible decay, we can set $m = 3$; therefore

$$N_\lambda = \frac{L_{max}}{\lambda_P} = \frac{V^2}{4\pi^2 m \cdot f_P \cdot D} \quad (16)$$

In eqn (16), N_λ specifies the maximum filter order realizable. The diffusion coefficient is also a function of velocity. The effective Taylor-dispersion adjusted diffusion coefficient D_{eff} can be approximately expressed as[23]

$$D_{eff} \cong \frac{\alpha(w,h)V^2}{D_0} \quad (17)$$

where a is a function of the width w and height h of the microfluidic channel[23,24]

$$\alpha(w,h) \cong \frac{1}{210}\left[\frac{8.5h^2w^2}{h^2 + 2.4hw + w^2}\right] \quad (18)$$

and D_0 is the intrinsic diffusion coefficient. In our case, D_0 for fluorescein disodium[28] is 8.2×10^{-10} m^2 s^{-1}. Substituting eqn (17) into eqn (16) we find the relationship between N_λ and f_P is

$$N_\lambda = \frac{D_0}{4\pi^2 m \cdot f_P \cdot \alpha(w,h)} \quad (19)$$

which to first order is independent of velocity. Fig. 5 shows a plot of N_λ *versus* f_P for 25 μm-wide channels of different heights. For any practical sharp filter, we need $N_\lambda \geq 5$. These two contraints define the boundary of the shadowed design feasibility region. Any feasible filter design must operate in this region. In a filter design procedure, we can first set a desired N_λ and f_P, and select h, such that the design maps inside the feasible design region.

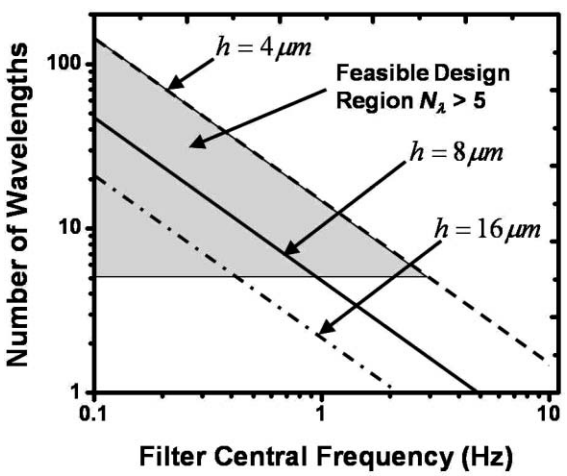

Fig. 5 Feasible filter design region for different channel heights.

With these initial choices we can now determine the flow velocity, wavelength and the maximum channel length which ultimately determines the chip size. The relation between flow velocity V and drive pressure P is

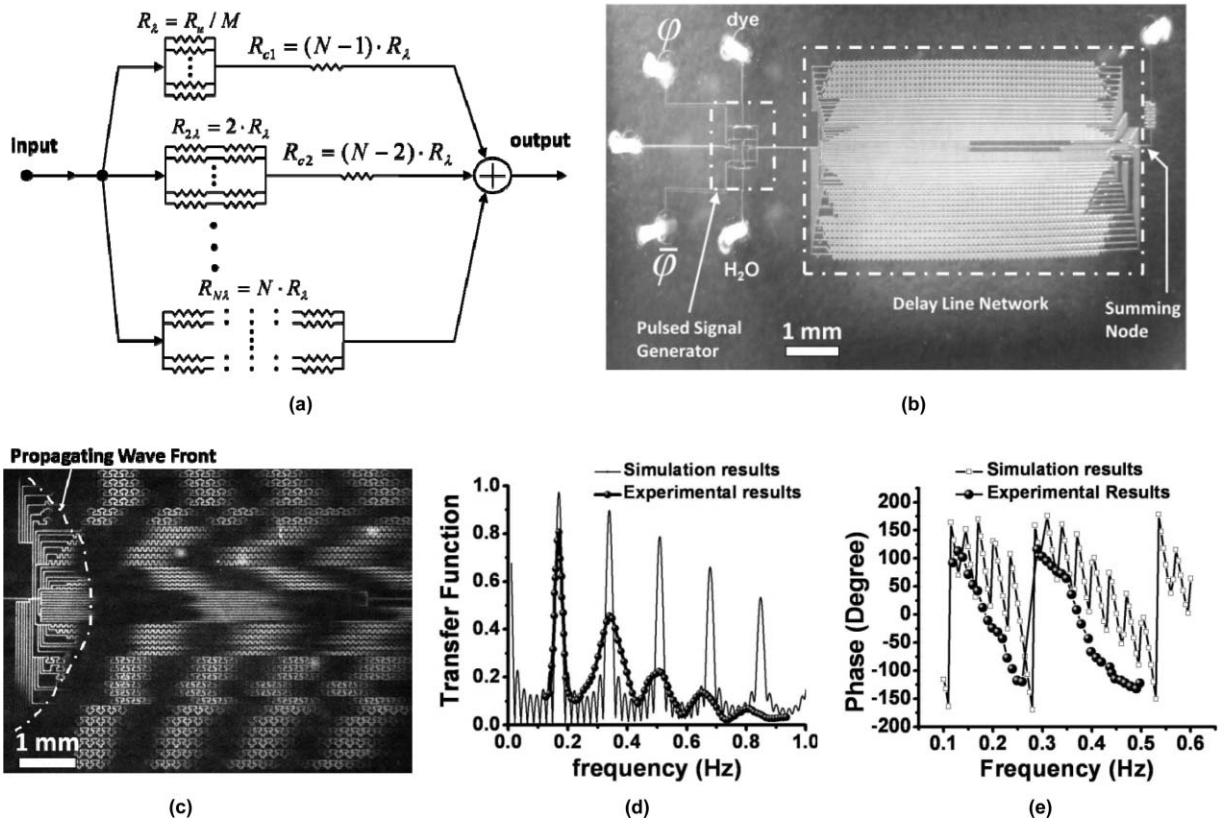

Fig. 6 (a) Schematic of a practical bandpass filter implementation. (b) Chip photo of an 8th order bandpass filter and signal generator with $M = 6$. The chip is 0.72 × 2.5cm^2. The flow channel cross section of this chip was 25 × 6 μm^2. At a flow rate of 6 mm s^{-1}, this chip has a f_P of 0.17 Hz. (c) Fluorescein waves propagating through the bandpass filter branches. The waves travel from left to right at $f = 0.4$ Hz and $V = 2.4$ mm s^{-1}. The dashed line indicates a propagating wave front. (d) Calculated and measured TF magnitude of the bandpass filter. The measurement spot was 25 × 25 μm^2. (e) Phase characteristics of the bandpass filter TF.

$$V = \frac{P}{\rho_f \cdot L_{max}} = \lambda_P \cdot f_P \tag{20}$$

where the flow resistivity ρ_f is a function of w and h and fluid viscocity μ, and

$$L_{max} = N_\lambda \cdot L = N_\lambda \cdot \lambda_P = \left(\frac{N_\lambda \cdot P}{\rho_f \cdot f_P}\right)^{1/2} \tag{21}$$

The relationship between eqn (19) and (21) thus specify all the parameters for the filter, and $N_\lambda \equiv N$ is exactly the filter order.

The feasible frequency range for the filter depends on many parameters. For typical chip dimensions and flow velocities it is possible to implement filter chips that discriminate signals with periods of a few seconds to several minutes.

Bandpass filter implementation

The ideal filter structure shown in Fig. 6 requires equal branch flows. This requirement cannot be met with a single driving pressure source because their branch channel lengths and corresponding flow resistances are different. However, we can approximately meet this requirement if we add a series flow resistor that equalizes the branch resistance but contributes minimally to the branch phase. Fig. 6(a) shows the schematic of a practical implementation of this idea. The filter chip consists of a microfluidic network with N branches, each branch composed of a delay line resistor $R_{i\lambda}$ and series compensating resistor R_{ci}.

Each delay line resistor consists of M channels of unit resistance R_u connected in parallel with overall resistance $R_{i\lambda} = i\cdot R_u/M$. In order to realize eqn (10) all branches must have the same total flow resistance R_b. Thus we have

$$R_b = R_{i\lambda} + R_{ci} = R_\lambda N \tag{22}$$

hence the compensating resistor is

$$R_{ci} = (N-i)R_\lambda = \frac{(N-i)}{M} R_u \tag{23}$$

All the resistances are functions of the microfluidic channel dimensions and can be calculated from[29]

$$R_f = \frac{\rho_f L}{wh} = \frac{12\mu L h^4}{\left(\frac{w}{h}\right) - \sum_{m=0}^{\infty} \left(\frac{192}{\pi^5 (2m+1)^5}\right) \tanh\left[\frac{(2m+1)\pi w}{2h}\right]} \tag{24}$$

For the bandpass filter to work properly all the phase delay should originate from the delay resistor, but the compensating resistor also introduces a finite phase error. This phase error should be minimized or at least limited to a range (0–90°) that does not significantly impact the interference. If the unit delay and compensating resistors have the same cross section, the phase error is

$$\Delta\phi_i = 2\pi \frac{N-i}{M^2} \tag{25}$$

The square term in the denominator is the result of the larger velocity through the branch compensation resistor $V_c = MV$. In order to surpress the phase error a large M should be used. For example for a filter with $N = 8$ and $M = 6$, the maximum phase error is 70° at f_P. At the higher peaks the phase error is much larger; hence progressively broader peaks of reduced amplitude are expected in the filter TF.

Device fabrication

Bandpass filter chips have been constructed using a double-layer PDMS stamp process.[30,31] All fluidic channels were formed using silicon wafer micro-molds. Conventional photolithography was used to form mold features using Clariant AZ9245 photoresist. Due to the nature of this photoresist, the mold feature profiles are rounded on the top. Minimum-width channels were 25 μm wide at the channel bottom (determined by the mask resolution) and 6 μm high at the channel center. The channels in the second air control level, which is below the liquid flow channel level, were fabricated using Microchem SU-8, an epoxy based negative photoresist. The control channel profiles are rectangular with dimension of 175 μm wide and 32 μm high at the valve locations. The rounded configuration of the flow level channels ensures that the on-chip air valves can pinch the flow channel off completely.

Molds were then spin coated with a thin layer of diluted detergent to facilitate mold release. After that, well mixed and degased silicone elatomer (Dow Corning Sylgand 184) was poured onto the liquid flow channel mold sitting in a plastic petri dish. For the air control channel, silicone elastomer was spun coated onto the mold. The spin speed was carefully chosen to be 1500 rpm for 1 min, which determined the thickness of the control channel and the active membrane. The thickness of the fluid flow channel was several milimeters to ascertain robust connections between the chip and tubings. The assembled chip can sustain a drive pressure up to 30 psi without leakage.

Both layers are cured in an oven for 3 h at 80 °C. Then the connecting holes were formed using a simple and effective microdrill process (Cameron Microdrill Press model 2A and ~600 μm diameter bits, McMaster Carr Ltd.) on the peeled off fluidic channel layer. Microdrilling was followed by a nitrogen blast that clears any debris from the PDMS surface. Bonding between the fluidic and control layer was achieved by reactivating the PDMS surface with oxygen plasma (March Instrument Inc.). Microscope arrangement (VZM 1000 Edmond Optics) was also used to asist alignment of the two layer. The assembled device was then peeled off the control channel mold and bonded to a precleaned glass substrate.

Fig. 6(b) shows an example 8th order bandpass filter chip and signal generator with $f_P = 0.17$ Hz at a flow rate of 1.4 mm s^{-1}. The chip shown consists of an array of 55 channels (6 per branch, 8 branches and 7 compensation channels) converging at a common output channel. The chip dimension is 7 mm × 25 mm with $L = 8$ mm and maximum channel length of 6.4 cm. The output of the summing node is followed by a mixing resistor. In the mixing resistor, the output flow velocity is $MNV = 48V$, much larger than that at each branch. The branch signals are therefore mixed quickly due to the much larger effective diffusion coefficient from eqn (17).

Experimental results

Experimental setup

Filter chips were tested using fluorescein disodium salt (Fisher, 1 mg mL^{-1} in water) as indicators of chemical concentration. Fluorescent intensity was measured for the fluorescein tracer dye at different concentrations in DI water. A linear dependence of fluorescence on fluorescein concentration was obtained. Flow lines of dye and water were connected to the input chip *via* syringe tubing (Small Parts TGY-010) with id of 0.010 inch and od of 0.030 inch pressure fitted into ~600 μm drilled chip inlets and outlets. Connections to hypodermic syringes were established by insertion of luer-fitted 60 gauge-needles into the tubing. The syringes were driven by air pressure at 15 psi in order to generate the internal chip flows. The PDMS valve control lines were driven with a USB-computer controlled (Ontrak ADU208) relay box electrically connected to a set of high pressure electromechanical valves (STC Valve 2P025 1/8″). The PDMS valves were pneumatically activated with an activation pressure of ~50 psi.

The fluorescent intensity of the output chemical signals, representative of time-dependent concentration, was recorded with an Olympus MVX10 epifluorescence microscope equipped with an Hamamatsu Orca C9100–01 intensified camera. All quantitative measurements of the image intensity were obtained using the Olympus Wasabi imaging software package. All fluorescence images were recorded with a sampling rate of ~15 ms.

Dynamic response measurement

We have measured the dynamic repsonse of the filter under different frequency excitation. Fig. 6(c) shows a fluorescent image of fluorescein waves propagating through the bandpass filter. As the excitation frequency increases, the wavelengh of the analyte becomes shorter. The transfer function and frequency response of the filter were extracted from the intensity data collected at the outlet of the chip. For a given excitation frequency, the signal amplitude at the fundamental frequency was obtained from the Fast Fourier Transform (FFT) of intensity data collected from 2000 consecutive images recorded at that frequency. Fig. 6(d) shows the experimental magnitude of the transfer function compared to the calculated value inclusive of attenuation. For the bandpass filter chip under test compared to the calculated values from eqn (9). The TF displays multiple peaks at 0.17, 0.34, 0.51 Hz, yielding $f_P/\Delta f_P \approx 4.2$, consistent with the calculated results.

The phase characteristics are also shown in Fig. 6(e). In general, the experimental peak amplitudes are broader than those calculated. This is most likely due to the presence of a larger dispersion than expected as well as the phase errors in the compensation resistors. Nevertheless, the sharp characteristics of this type of filter permit us to selectively separate specific input frequencies at the filter output with a high degree of rejection for out of band signals.

Summary

We presented a new experimental technique for the separation of dynamic chemical signals based on their Fourier frequency domain characteristics. Such technique can be used to create filters that separate slow signals from fast signals from a common input flow stream. We developed mathematical models and a set of simple experiments that demonstrate that short microfluidic channels behave as linear delay lines. Such delay components can be utilized to implement frequency dependent interference filters. Using these models we designed, fabricated and tested a PDMS-based Fourier domain bandpass filter. These PDMS filter modules can be integrated with other PDMS based microfluidic components to form more complex chemical analysis systems. For typical chip dimensions and flow velocities it is possible to implement filter chips that discriminate signals with periods of a few seconds to several minutes.

References

1 W. R. Loewenstein, *The Touchstone of Life*, Oxford, NY, 1999.
2 D. Niehoff, *The Language of Life: How Cells Communicate in Health and Disease*, National Academic Press, NY, 2006.
3 J. T. Hanckock, *Cell Signalling*, Prentice Hall, NY 1997.
4 Lodish *et al.*, *Molecular Cell Biology*, Freeman, NY 2001.
5 D. A. Lauffenburger and J. L. Linderman, *Receptors: Models for Binding, Trafficking, and Signaling*, Oxford, NY 1993.
6 H. Gutfreund, *Kinetics for the Life Sciences*, Cambridge Press, NY 1995.
7 B. Schoeber *et al.*, *Nat. Biotechnol.*, 2002, **20**, 370–375.
8 B. N. Kholodenko, *Nat. Rev. Mol. Cell Biol.*, 2006, **7**, 165–176.
9 P. G. P. Nucifora and A. P. Fox, *J. Neurosci.*, 1999, **19**, 9739–9746.
10 B. O. Palsson and S. N. Bhatia, *Tissue Engineering*, Prentice-Hall, NY 2004.
11 J. Angleson and W. Betz, *Trends Neurosci.*, 1997, **20**, 281–287.
12 J. Sorensen, U. Matti, S. Wei, R. Nehring, T. Voets, U. Ashery, T. Binz, E. Neher and J. Rettig, *Proc. Natl. Acad. Sci.*, 2002, **99**, 1627–1632.
13 Q. Zhang, M. Tally, O. Larsson, R. Kennedy, L. Huang, K. Hall and P. Berggren, *Proc. Natl. Acad. Sci.*, 1997, **94**, 6232–6237.
14 R. M. Seymur and B. Henderson, *IMA J. Math. Appl. Med. Biol.*, 2001, **18**, 159–192.
15 R. F. Batgaze, *et al.*, *J. Exp. Med.*, 1994, **180**, 1785–1792.
16 D. Irimia, *et al.*, *Lab Chip*, 2006, **6**, 191–198.
17 L. Wolpert, *et al.*, *Principles of Development*, Oxford, NY 2002.
18 Y. Kwok and A. Manz, *J. Chromatogr., A*, 2001, **924**, 177–186.
19 S. Kitagawa, K. Mitsuya, C. Chaiyasut and T. Tsuda, *J. Sep. Sci.*, 2003, **26**, 1169–1174.
20 X. Yang, G. Jenkins, J. Franzke and A. Manz, *Lab Chip*, 2005, **5**, 764–771.
21 P. Auroux, D. Iossifidis, D. Reyes and A. Manz, *Anal. Chem.*, 2002, **74**, 2637–2652.
22 N. Nguyen and X. Huang, *Lab Chip*, 2005, **5**, 1320.
23 D. A. Beard, *J. Appl. Phys.*, 2001, **89**, 4667–4669.
24 D. Dutta and D. T. Leighton, Jr., *Anal. Chem.*, 2001, **73**, 504–513.
25 D. Dutta, A. Ramachandran and D. T. Leighton, Jr., *Microfluidics Nanofluidics*, 2006, **2**, 275–290.
26 A. Ajdari, N. Bontoux and H. A. Stone, *Anal. Chem.*, 2006, **78**, 387–392.
27 N. Bontoux and H. A. Stone, *Anal. Chem.*, 2006, **78**, 387–392.
28 J. R. Saylor and K. R. Screenivasan, *Phys. Fluids*, 1998, **10**, 1135–1146.
29 W. E. Marf, *et al.*, *Sens. Actuators, B*, 2001, **72**, 266–272.
30 M. A. Unger, H. P. Chou, T. Thorsen, A. Acherer and S. R. Quake, *Science*, 2000, **288**, 113.
31 L. Chen, F. Azizi and C. H. Mastrangelo, *Lab Chip*, 2007, **7**, 850–855.